# Spatiotemporal measurements of striations in a glow discharge's positive column using laser-collisional induced fluorescence

Z. K. White **2** (0); R. P. Gott (0); B. Z. Bentz (0); K. G. Xu (0)

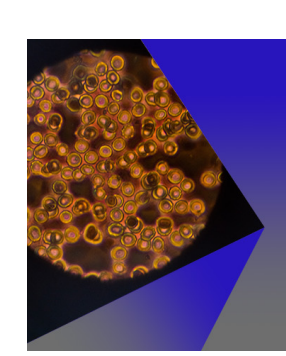


AIP Advances 13, 085015 (2023) https://doi.org/10.1063/5.0096695





CrossMark



# **AIP Advances**

Special Topic: Medical Applications of Nanoscience and Nanotechnology

**Submit Today!** 



# Spatiotemporal measurements of striations in a glow discharge's positive column using laser-collisional induced fluorescence

Cite as: AIP Advances 13, 085015 (2023); doi: 10.1063/5.0096695 Submitted: 20 April 2022 • Accepted: 26 July 2023 • **Published Online: 9 August 2023** 















# **AFFILIATIONS**

- <sup>1</sup> Mechanical and Aerospace Engineering Department, The University of Alabama in Huntsville, Huntsville, Alabama 35899, USA
- <sup>2</sup>NASA Postdoctoral Program, Merritt Island, Florida 32899, USA
- <sup>3</sup>Sandia National Laboratories, Albuquerque, New Mexico 87185-1423, USA

#### **ABSTRACT**

We have observed the behavior of striations caused by ionization waves propagating in low-pressure helium DC discharges using the noninvasive laser-collision induced fluorescence (LCIF) diagnostic. To achieve this, we developed an analytic fit of collisional radiative model (CRM) predictions to interpret the LCIF data and recover quantitative two-dimensional spatial maps of the electron density,  $n_e$ , and the ratios of LCIF emission states that can be correlated with  $T_e$  with the use of accurate distribution functions at localized positions within striated helium discharges at 500 mTorr, 750 mTorr, and 1 Torr. To our knowledge, these are the first spatiotemporal, laser-based, experimental measurements of  $n_e$  in DC striations. The  $n_e$  and 447:588 ratio distributions align closely with striation theory. Constriction of the positive column appears to occur with decreased gas pressure, as shown by the radial  $n_e$  distribution. We identify a transition from a slow ionization wave to a fast ionization wave between 750 mTorr and 1 Torr. These experiments validate our analytic fit of  $n_e$ , allowing the implementation of an LCIF diagnostic in helium without the need to develop a CRM.

© 2023 Author(s). All article content, except where otherwise noted, is licensed under a Creative Commons Attribution (CC BY) license (http://creativecommons.org/licenses/by/4.0/). https://doi.org/10.1063/5.0096695

#### I. INTRODUCTION

The stratification, or alternating dark and light regions, of the positive column in a DC discharge is a well-known phenomenon studied both experimentally and theoretically over the last two centuries. In the positive column, striations can appear as either stationary or moving bright regions of plasma in either molecular or inert gases. The positive column is the region of the glow discharge extending from the anode. In inert gases, striations usually move at high speeds and cannot be seen by the naked eye. The appearance of striations is due to ionization waves within the plasma. These ionization waves can be described as "backward" waves when the phase velocity and group velocity are directed in different directions. These backward waves usually appear in striated inert gas discharges. Extensive reviews were completed in the late 1960s through the 1980s on striations' theoretical and experimental

progression.<sup>1-3</sup> Pekarek<sup>1</sup> described the physical mechanism of striations as induced by a local perturbation of the ion and electron density within the plasma that spurs the observed oscillatory process. The initial perturbation, e.g., an applied pulsed voltage, can cause a local increase in ion and electron density, giving rise to a decrease in temperature. This decrease in temperature is a space-charge effect caused by the different mobilities of the ions and electrons. As more mobile electrons attempt to leave a given region, an electric field arises to slow them to preserve quasineutrality, thus decreasing the electron temperature. As the electron temperature decreases, the ionization rate also decreases, resulting in a drop in charged particle density. As the density drops, the electric field initially slows down the electrons, allowing them to regain their energy. As the electrons increase in temperature, the ionization rate also increases and once again creates a region of increased ion and electron density, thus repeating the process.

a) Author to whom correspondence should be addressed: zw0015@uah.edu

How the onset of striations occurred was of practical interest in applications such as gas discharges, He-Ne gas lasers, and semiconductor etching. The experimental work on striations consisted of observations and measurements of the plasma using various methods such as microwave absorption, 4,5 Langmuir probes, 6-8 and rotating mirrors.9 Pekarek1 reviewed an expanse of experimental work covering the types of waves, the artificial onset of striations due to an external perturbation, the behavior of ionization waves in inert gases, and the behavior of molecular gases such as hydrogen and oxygen. More recently, Kolobov<sup>10</sup> wrote a review that focused on the discovery of striations in constricted discharges, the electron kinetics in spatially inhomogeneous plasmas, and computational modeling at multiple operating conditions. Further work modeling striations has also been done. 11-14 The review performed recently by Golubovskii et al.15 analyzed the studies on electron kinetics in spatially periodic fields such as striated discharges by performing electron energy distribution function (EEDF) analysis. The importance of electron kinetics in low pressure, low current discharges such as the one used in our study is described more indepth in the references. 16-18 Golubovskii et al. 19 obtained detailed two-dimensional plasma-induced emission maps of the constriction and formation of moving striations in a discharge tube. Another study<sup>20</sup> used planar laser-induced fluorescence to measure the spatiotemporal distributions of helium atoms in 2<sup>3</sup>P. Still, no measurements of electron density or electron temperature were done using two-dimensional, noninvasive techniques.

The current study focuses on characterizing the complete lifetime of the positive column's stratification by obtaining temporally and spatially resolved two-dimensional maps of electron density ( $n_e$ ) and specific collisional excitation states that are dependent on  $T_e$ within the plasma using the laser-collisional induced fluorescence (LCIF) diagnostic method. The use of laser-excited states compared to just plasma-induced emission gives us a complete picture of the behavior occurring within the tube. For example, we measured the phase shift between  $n_e$ , the ratio between the 447 and 588 LCIF emission states, the light intensity, and the radial constriction of  $n_e$  with decreasing pressure. Experimental measurements of the phase shift between  $n_e$  and  $T_e$  have been shown before, although with Langmuir probes. Previous studies  $^{20-24}$  have shown the advantages of using a non-invasive laser diagnostic to characterize a noble gas discharge. To the best of our knowledge, no other experimental work has obtained two-dimensional spatiotemporal measurements of  $n_e$  in striations with the possibility of being extended to  $T_e$ .

#### II. EXPERIMENT

The DC plasma used in this experiment was generated in a 47 cm long, 4 cm inner diameter glass tube connected on either side to a stainless steel KF 40 cross, as shown in Fig. 1. On the ends of these crosses were CF-viewports with quartz windows to allow the laser beam to pass through the tube. A dry scroll pump was used to evacuate the air from one end of the tube, and high purity helium flowed into the system at the opposite end. The background pressure of the tube is ~100 mTorr before the Helium is present. A needle valve on the vacuum pump line and the mass flow controllers were used to control the working pressure. Helium was chosen due to its long-lived metastable states compared to other noble gases and the established ability to determine  $n_e$  and effective  $T_e$  from helium LCIF measurements using a collisional-radiative model (CRM).<sup>21</sup> The stainless-steel crosses on the tube ends were used as electrodes to maximize the electrode surface area and minimize parasitic discharges and sputtering. Ballast resistors were used to further prevent the discharge from arcing. A potential difference of 750 V and a constant current of 28 mA were applied to the electrodes at helium pressures close to 500 mTorr. To ignite the plasma discharge, a commercial plasma ball was placed close to the tube. The resulting discharge consisted of a positive column that spanned the length of the tube, with the cathode glow region being barely visible and lying within our hollow cathode.

A key objective of the experiment was to spatially synchronize the striations with the laser pulse. This was done by overlaying a 2.5 kV,  $10 \mu$ s wide square wave pulsed voltage on top of the steady

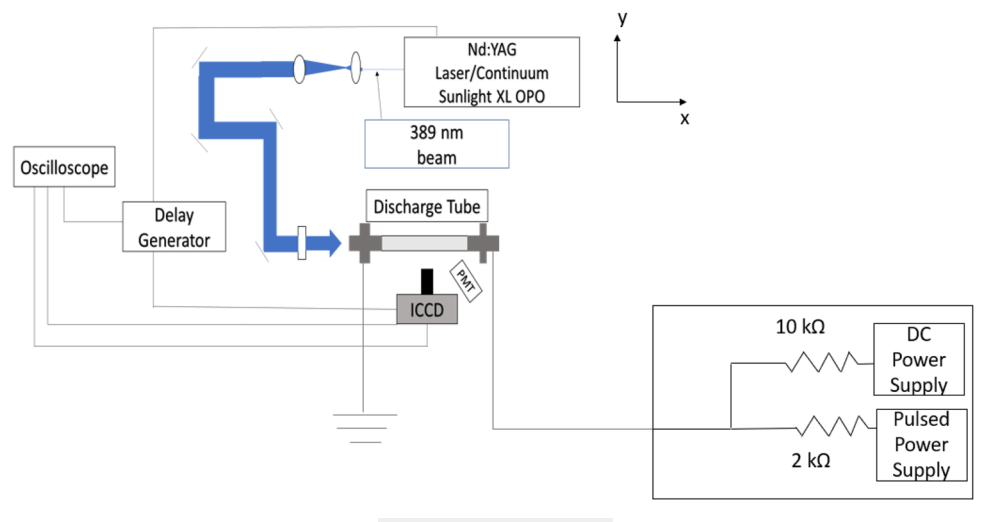
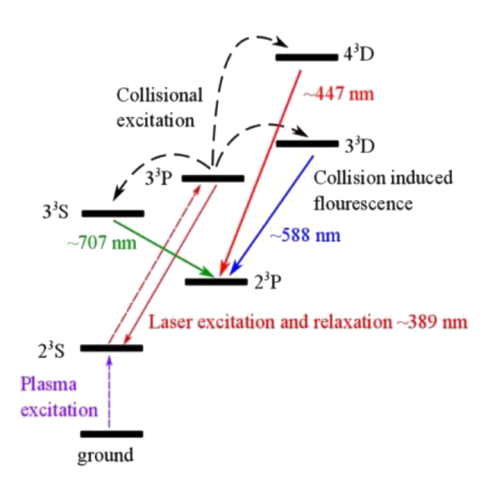


FIG. 1. Experimental setup.

DC voltage. The high voltage pulse "reset" the striations and enabled the repeatable formation of ionization waves over several hundreds of  $\mu$ s, depending on the specific operating condition, after the high voltage pulse. The discharge before the pulse consisted of irregular low light intensity striations at the anode and a steady-state plasma near the cathode. A photomultiplier tube captured the light intensity within the tube to measure the appearance of the striations, which were displayed on a Waverunner 6200 oscilloscope. An Andor iStar 334-T ICCD camera with a 200-800 nm spectral range was positioned perpendicular to the tube and laser path. The size of the optical table and our interest in the behavior of the discharge near the electrodes limited the field of view of our camera. The camera delay was set to specific times after the pulse to capture the timeresolved phenomena within the striations. The camera gate width was set to 30 ns, and five images were averaged to make each LCIF image. We did not account for the dispersion effects related to the thickness of the tube wall. The assumption was made that the quartz tube has minimal absorption and dispersion of the wavelengths of interest. Given the distance of the camera, any dispersion is likely only a few pixels of shift, which would have a minimal effect on the 2D maps. Bandpass filters with center wavelengths of 590, 450, and 390 nm (±10 nm FWHM) were used to capture the desired helium LCIF emissions. A 389 nm collimated laser beam focused into a light line with a width of <1 mm at the focal length and 3.6 mm at the edges, along the central axis of the tube, was used to excite the He atoms in the plasma from the metastable 23S state to the 33P state, as shown in Fig. 2. The 3<sup>3</sup>P state atoms undergo collisions with free electrons that cause redistribution to the 3<sup>3</sup>S, 3<sup>3</sup>D, and 4<sup>3</sup>D states. The relaxation of the laser-excited and neighboring collision excited states results in the emission of photons at 389 nm (3<sup>3</sup>P to 2<sup>3</sup>S), 588 nm (3<sup>3</sup>D to 2<sup>3</sup>P), and 447 nm (4<sup>3</sup>D to 2<sup>3</sup>P) that are captured by the ICCD camera. The 707 nm (3<sup>3</sup>3 to 2<sup>3</sup>P) state is independent of the 389 nm (3<sup>3</sup>P to 2<sup>3</sup>S) state; therefore, it is not used in the calculation of parameters. For each measurement, the camera acquires two sets of images: one at the set delay after the laser pulse and one 500 ns before the laser pulse. The first set captures the LIF (at 389 nm) or



**FIG. 2.** Illustration of LCIF in helium. Measurements of the laser excited 389 nm emission and the collision excited 447 and 588 nm emissions allow the determination of  $n_e$  and effective  $T_e$ .

LCIF (at 588 and 447 nm) plus plasma-induced emission. The second set captures just the plasma-induced emission (at 389, 588, and 447 nm). The plasma-induced emission images were subtracted to produce the final LIF or LCIF images.

The data were acquired using a LabView routine that was interfaced with the camera via a universal serial bus (USB) port. The stored data were then post-processed in MATLAB to produce 588:389 and 447:588 nm intensity ratio images. These ratios can be used to determine the  $T_e$  and  $n_e$  within the region of the plasma excited by the laser light sheet using a collisional-radiative model (CRM).<sup>21</sup> The CRM solves a system of differential equations that describe changes in atomic state densities due to electronic, photonic, and atomic driven processes. Collision-induced state transition rates were calculated from interaction cross-sections assuming a Maxwellian electron velocity distribution defined by  $T_e$ . The CRM neglects interactions that can cause electron states to transfer to the singlet and triplet stats, and only states in the triplet manifold up to n = 5 are considered. Using the Einstein coefficients, the LIF and LCIF 588:389 and 447:588 nm intensity ratios caused by the laser light pulse can be calculated for the specified  $T_e$  and  $n_e$  to interpret the experimental measurements. In the use of the 3<sup>3</sup>P and 3<sup>3</sup>D states to calculate the  $n_e$ , the presence of a non-Maxwellian EEDF has no effect because of the small energy spacing between these two transitions. This point is key because the EEDF in striated glow discharges is known to be non-Maxwellian, specifically having a bimodal distribution. The independence of the EEDF cannot be said about the rates used to calculate the  $T_e$ , which has been previously referred to as an "effective" temperature,  $T_{\rm eff}$ . Deviations from a Maxwellian distribution will complicate the quantitative determination of electron temperatures. This effect is most pronounced when there is a significant population of high energy electrons, as in a drifting Maxwellian or beam-like distribution or, as mentioned, the bi-modal distributions seen in striated glow discharges. The results are, therefore, presented as  $T_e$  sensitive 447:588 LCIF ratio images. In the Appendix, we introduce an analytic fit generated from the CRM that can be used to convert the intensity ratios to  $T_{\rm eff}$  and  $n_e$ . This fit was applied at each camera pixel to form 2D images of  $T_{\text{eff}}$  and  $n_e$ , where we assume a constant electric field within a pixel. The image data were thresholded to omit any background data that appeared outside the boundaries of the tube. The threshold was set at the maximum signal value appearing outside of the tube to eliminate any data appearing outside of the tube. Any data below this threshold inside the tube was also eliminated and considered to be background noise or a product of scattering or reflections. Section III will provide an overview of the data produced by our study.

# III. RESULTS

# A. Group and phase velocities

The discharge was imaged at different pressures and at different times after the high voltage pulse. Temporal sweeps of  $\sim 1$  ms with  $10~\mu s$  time steps were performed for various pressures to determine an upper pressure bound. At pressures above 1 Torr, the striations became inconsistent from pulse to pulse, which prevented repeatable measurements. Therefore, no results were obtained at pressures higher than 1 Torr. This may be attributed to multiple wave types being excited simultaneously. The 1 Torr, 750 mTorr, and 500 mTorr cases exhibited clear transitions from a non-striated

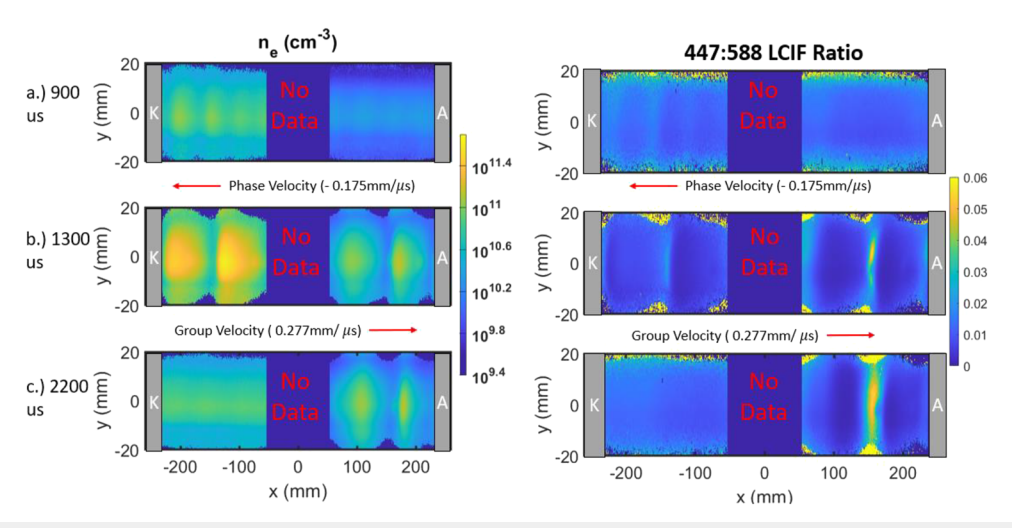


**FIG. 3.** Maps of  $n_e$  and the 447:588 LCIF ratio measured in the 1 Torr discharge at (a) 900, (b) 1300, and (c) 2200  $\mu$ s. The Striations propagate from the anode (A) to the cathode (K) at the specified phase velocity. The bulk motion of the plasma at the group velocity is from the cathode to the anode. No data were measured in the region from x = -55 mm to x = 55 mm.

discharge to a stratified discharge and back again. For these three pressures mapped, over the entire lifetime of the striated discharge, only three or four distinct striations propagated across the tube. Figures 3–5 show the stratification process of the discharge at the anode and cathode regions of the tube for the 1 Torr, 750 mTorr, and 500 mTorr cases, respectively. Due to the limited field of view of the camera, the middle of the tube between x=-55 mm and x=55 mm was not captured. The phase velocities measured by the propagation of the striated structures from the anode to the cathode and the group velocities measured by the bulk motion of the plasma from the cathode to the anode are shown in Figs. 3–5. Within our coordinate system, the velocities are positive if moving from left to right. The following subsections will go over the basic behaviors

readily observed throughout all three pressures and the unique behaviors at each pressure.

## B. Wave propagation phenomena

The basic motion of the striations can be tracked by following the change in density from one image to another. As stated earlier, the onset of the ionization wave is induced by the application of a voltage pulse. There is a different lag time between the voltage pulse and the first appearances of the wave in the tube at different pressures, causing the different initial time steps of 900, 900, and 600  $\mu$ s for the 1 Torr, 750 mTorr, and 500 mTorr cases shown in Figs. 3–5. The appearance of the ionization wave is marked by the formation

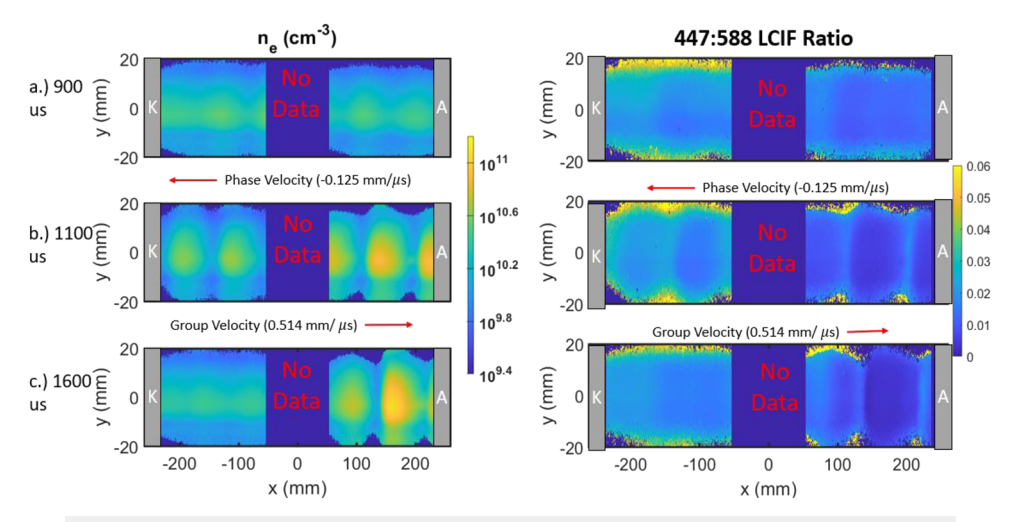


**FIG. 4.** Maps of  $n_e$  and 447:588 ratio measured in the 750 mTorr discharge at (a) 900, (b) 1100, and (c) 1600  $\mu$ s.

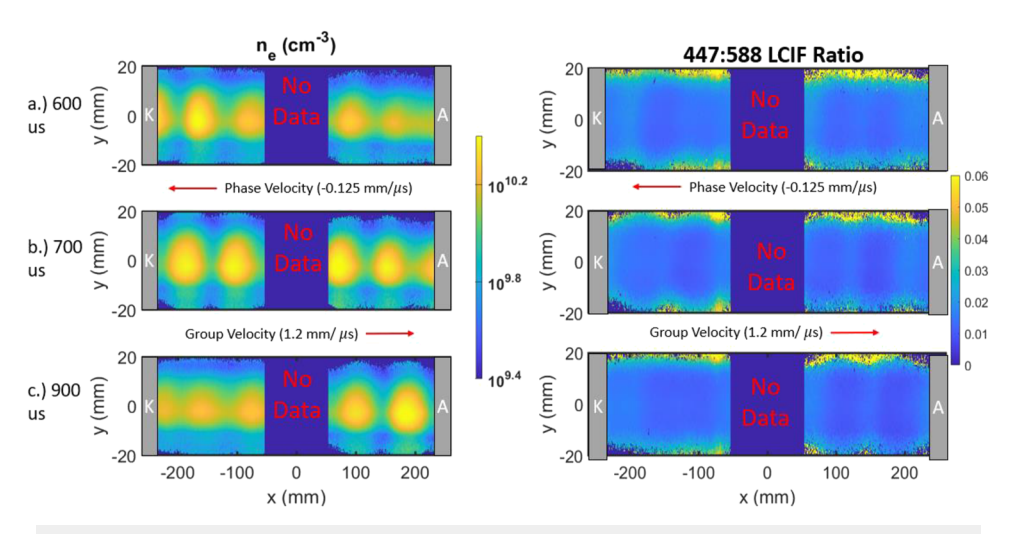
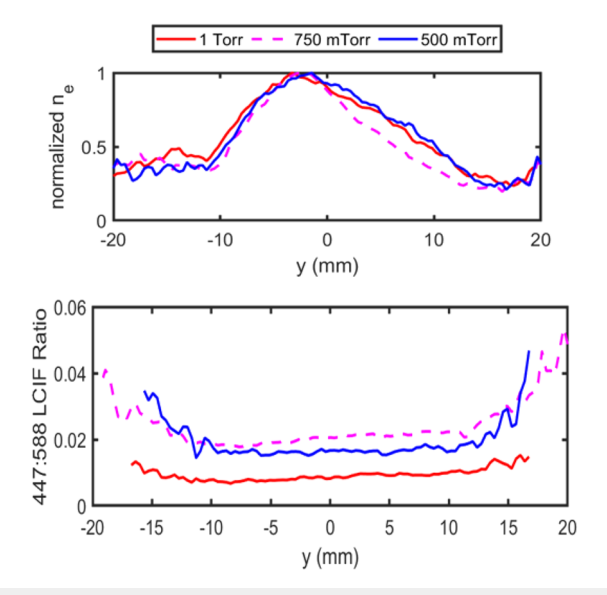


FIG. 5. Maps of  $n_{\rm e}$  and the 447:588 LCIF ratio measured in the 500 mTorr discharge at (a) 600, (b) 700, and (c) 900  $\mu$ s.

of striated structures in the cathode and anode regions. Considering the 1 Torr case, the ionization wave first appears in the cathode region and then propagates to the anode region, showing that the group velocity is directed from the cathode to the anode. At the last time point, the striations in the cathode region either disappear, as in Figs. 3 and 4, or are elongated, as in Fig. 5. At this moment, we assume that the ionization wave excited by the voltage pulse has transitioned out of the cathode region and exists exclusively in the anode region, where striated structures are still visible. Beyond the final time point shown in the figures, the entire discharge tube transitioned into a pre-pulse state where the cathode region was near homogeneous and the anode region contained irregular low light intensity striations. It is important to note that in Figs. 3-5, the individual phases do not always exhibit backward wave behavior. In the supplementary material, we have included an animated video of the 389 nm emission propagating through the tube, which clearly shows that the striations are of the backward wave variety but exhibit oscillatory behavior around particular phases. The discharge was held in this state until another voltage pulse initiated the next ionization wave.

Figure 6 shows the radial distribution along the center of a striation at each of the three pressures. The radial distributions are somewhat asymmetric, and their shape at each pressure is similar. The  $n_e$  distributions show little to no shrinking as the pressure decreases, but the 447:588 ratio distributions show that there is a high 447:588 region forming near the walls at 750 and 500 mTorr. It appears that a space-charge sheath is growing here, which may occur before the  $n_e$  distribution shows signs of constriction. Within the sheath, there is also a spatial oscillation of the parameters. We discuss this in Sec. IV B.

Considering Fig. 3, there is a clear increase in the 447:588 ratio in the anode region that does not appear in the cathode region or in Fig. 4 or Fig. 5. Furthermore, the spatial region containing this high 447:488 ratio is smaller in Fig. 3 compared to Figs. 4 and 5. We discuss this in Sec. IV C.



**FIG. 6.** Radial distributions of  $n_{\rm e}$  and the 447:588 LCIF ratio along a radial slice of a striation at 1 Torr, 750 mTorr, and 500 mTorr. Near the wall, at 750 and 500 mTorr, the 447:588 ratio increases, while at 1 Torr, there is a smaller relative increase in the 447:588 ratio.

# C. Observed phase shift between $n_e$ and 447:588 LCIF ratio

An expected central phenomenon of striations is a phase shift between  $n_e$  and  $T_e$  that drives the propagation of the ionization wave. Figure 7 shows the axial distributions of  $n_e$ , the 447:588 LCIF ratio, the plasma induced emission, and the laser induced light intensity in the anode region at 500 mTorr. The light intensity is a 390 nm emission acquired before laser excitation. Comparing the  $n_e$  and 447:588

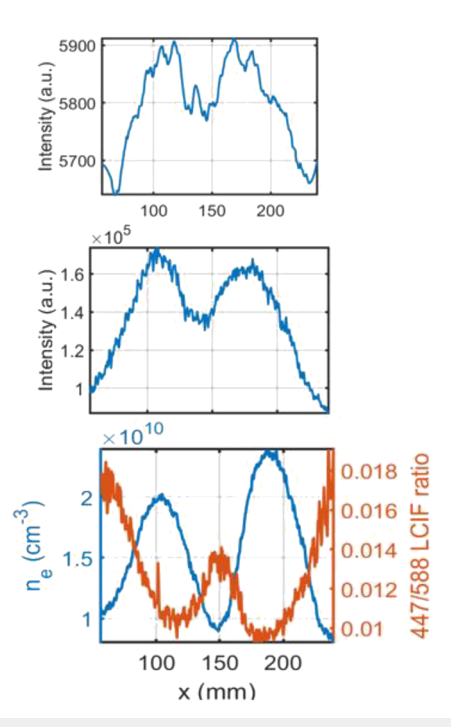


**FIG. 7.** Axial distributions of plasma emission intensity from 389 nm (top), laser induced intensity (metastable) from 389 nm (middle), and  $n_e$  and  $T_{\rm eff}$  (bottom) at the anode at 500 mTorr. The phase shift between  $n_e$  and the 447:588 ratio is apparent with LCIF but not plasma emission (the 447:588 ratio is phase-shifted toward the cathode).

LCIF distributions, we see that the 447:588 intensity ratio is shifted in the direction of the cathode. We also note that the light intensity distribution is only marginally in phase with the  $n_e$ . We discuss this further in Sec. IV A.

# **IV. DISCUSSION**

# A. $n_e$ , 447:588 ratio, and light intensity axial distributions

The striations in our experiment follow the theory laid out by Refs. 1-3 well. First, the observed ionization waves could be described as "backward" waves since the phase velocity was directed toward the cathode and the group velocity toward the anode. The theory describing the propagation of striations is covered in Refs. 1-3 and 10. They rely on the phase offset of  $T_e$ , which within our study could likely be in phase with the 447:588 ratio with respect to  $n_e$ , which is driven primarily by transport processes. The previous experimental literature suggested that light intensity lies nearly in phase with  $T_e$  and out of phase with  $n_e$ . <sup>4-6</sup> Referring to Fig. 7, we can see that this was not entirely true in our results. Here, the light intensity from the plasma induced emission and laser induced emission is slightly out of phase with the  $n_e$  and close to  $180^{\circ}$  out of phase with the 447:588 ratio. The differences observed in our study may be attributed to our "light intensity" measurements filtering out all but the 390 nm light and others measuring a broad spectrum of light from the discharge.

Recent simulation results <sup>11–13</sup> mostly align with the experimental results from our study. The simulated phase shift is closer to a quarter-cycle, while our results show a near half-cycle phase shift. The distributions shown in Fig. 7 confirm that the striation behavior can be predicted with simulation along the axis of our experimental setup. However, phenomena are occurring radially at all pressures that are worth further investigation, such as the asymmetry and constriction observed in Fig. 6.

#### **B.** Partial constriction

A diffuse discharge could be identified as plasma covering the entire radius of the tube, while a constricted discharge would show the plasma beginning to occupy less area radially. We believe that the 500 mTorr, 750 mTorr, and 1 Torr cases all show slight constriction. Viewing the computational results from Ref. 13, we see that the space-charge sheath grows when the discharge is constricted. We believe that we have observed this effect in our data at 500 and 750 mTorr. The space charge sheaths observed in Fig. 6 are indicative of the discharge constricting on the axis. The observed oscillations also appear to oscillate at a similar frequency, which could mean that they are appearing because of sheath instability.

Traditionally, in glow discharges, increases in currents lead to a constriction of the discharge. We operated our experiments with a pulsed DC voltage that was held constant for each pressure. There-

**TABLE I.** Parameters of different wave types appearing throughout the different pressures in helium.

Pressure (Torr)	λ (mm)	V <sub>p</sub> (m/s)	V <sub>g</sub> (m/s)
0.5	81.2	-125	1200
0.75	91.7	-125	514
1	160.9	-175	277

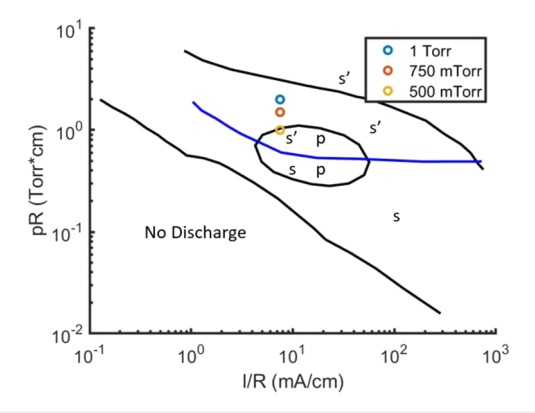


**FIG. 8.** pR vs I/R plot adapted from Ref. 27, including the points measured in our study. There was disagreement between our measured parameters, such as potential drop and phase velocity, and the location of our points on the plot. We believe that this discrepancy is because of the measurement of the ranges in a self-excited discharge in Ref. 27 and an externally excited discharge in ours. Reproduced with permission from V. Peřina, "Existence regions of ionization waves (moving striations) in helium, neon, and argon," Czech. J. Phys. B **26**(7), 764–768 (1976). Copyright 1976, Springer Nature.

fore, the current is expected to increase in the plasma at lower pressures, causing constriction of the discharge. Unfortunately, we did not record the current and voltage measurements and cannot confirm if this was the case.

# C. Observed wave transition from 750 mTorr to 1 Torr

Although an interesting observation, the possible constriction of the column does not explain why the plasma contained

condensed regions of high values of the 447:588 ratio at 1 Torr, as mentioned in Sec. III B. A possible explanation is an ionization wave-type change. The four most common ionization wave types observed in discharges are the fast s and r waves and the slow s' and p waves. However, only the s, s', and p waves have been observed in helium discharges. Therefore, it seems possible that we observed a transition from one wave type to another as the wave propagated. The different wave types are known to correspond to the kinetic resonances of the EEDF. <sup>26</sup>

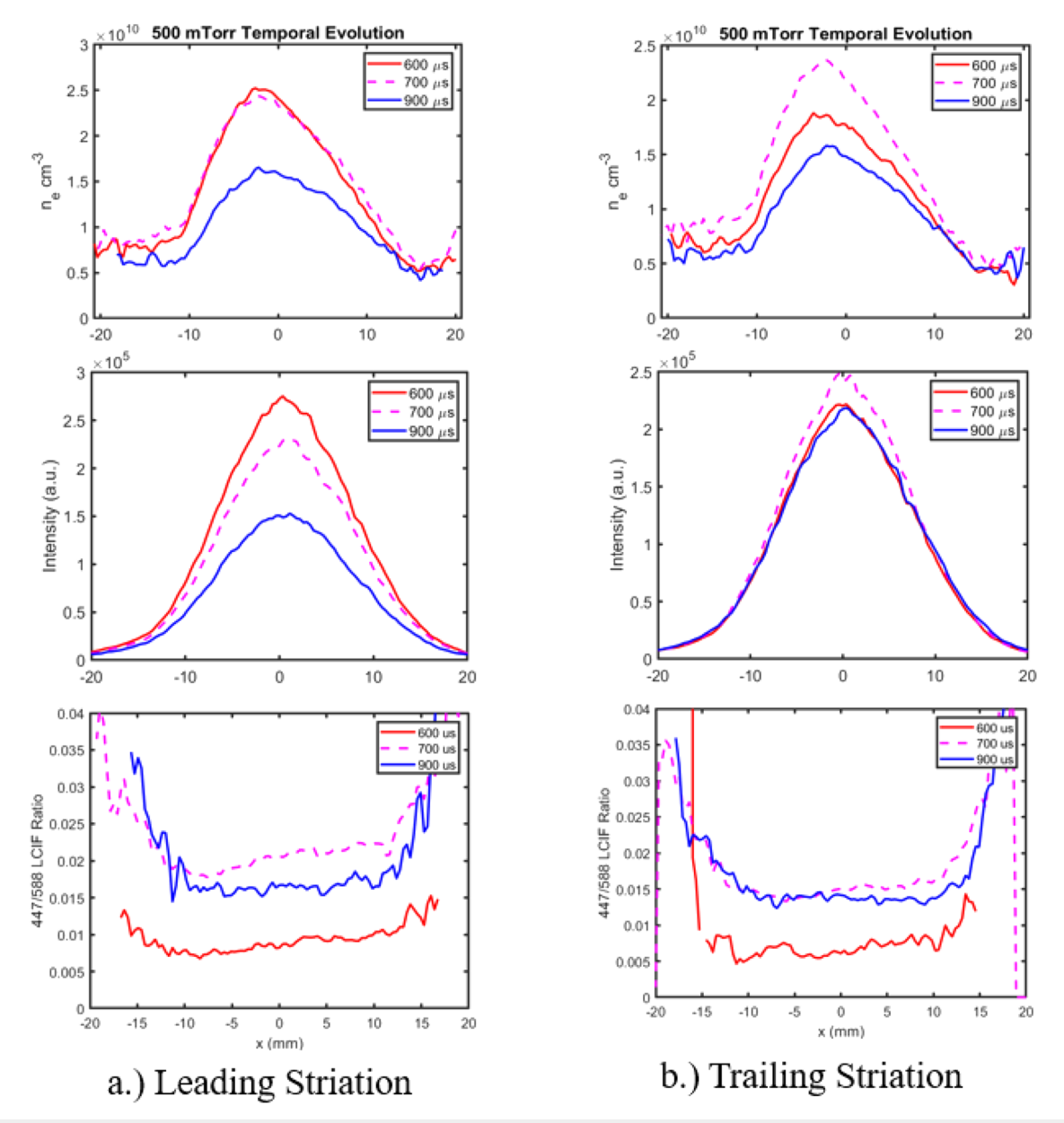


FIG. 9. Radial distributions of the electron density (top), laser induced intensity (middle), and the 450:590 ratio (bottom), respectively, measured over time at 500 mTorr. (a) Shows the leading striation and, (b) shows the trailing striation. Over each of the time steps, the rate of change of the 447:588 ratio increases closer to the wall, suggesting that the 500 Torr case is in a constant state of partial constriction.

A wave type transition can also be confirmed using the phase velocity. Fast-wave behavior shows that the phase velocity is proportional to the electric field, which may explain why the striations exhibited a higher phase velocity at 1 Torr. Slow-wave behavior has the opposite effect, such that when the electric field increases, the phase velocity decreases. Therefore, the fact that we measured approximately the same phase velocity for 500 and 750 mTorr gives us confidence that, within the operating conditions used, the wave existing at these pressures was of the slow p (q = 2 resonance) type. The increase in phase velocity in the 1 Torr case is consistent with the fast s (q = 1 resonance) wave's direct proportionality to the electric field.

The wavelength of the ionization wave and phase velocity at 1 Torr shown in Table I confirmed our suspicion that the pressure increase led to the q=1 resonance being excited. Peřina's<sup>27</sup> study on the existence of regions of spontaneously occurring striations in helium shows that the opposite result should happen, e.g., the move from 750 mTorr to 1 Torr should lead to a transition from a fast wave to a slow wave, as shown in Fig. 8. We believe the use of external excitation of the waves using an external voltage pulse causes changes in the existence regions  $f_0$  the particular ionization waves. How the overlaying of external voltages to excite the waves affects the propagation is worth further study.

# D. Spatial growth and decay

Figure 9 shows the  $n_e$ , metastable, and 447:588 ratio time evolution of the two visible striation peaks in the cathode region of the tube at 500 mTorr. In Fig. 9(a), we see the leading striation that is closer to the cathode. It holds a steady  $n_e$  peak from 600 to 700 us and then decays from 700 to 900 us. In Fig. 9(b), we see the trailing striation that is further from the cathode. In this case, the  $n_e$  peak grows from 600 to 700  $\mu$ s and then decays from 700 to 900 µs. Overall, the peaks in electron density are observed to decay as they propagate toward the trailing edge of the ionization wave packet and grow as they propagate toward the center of the ionization wave packet. This is consistent with the striations moving within the wave packet according to the measured phase and group velocities. The growth rate and decay also show that the discharge's partial constriction fluctuates as the wave packet propagates. This is consistent with observations of the high 447:588 ratio regions surrounding the discharge in cases where the wave packet has either not propagated or just passed through. In addition, the sheath instability seems to not appear when only measuring the metastable density, which could mean the instability is driven primarily by collisional processes. We also observe that the rate of change in the 447:588 ratio increases at positions closer to the tube walls, consistent with a space charge sheath that is growing due to the constriction of the discharge.

## V. CONCLUSION

We have performed LCIF measurements of  $n_e$ , laser, and collisional excited states in two-dimensions. The 447:588 ratio is a first approximation of how the  $T_e$  is possibly behaving, and pairing the LCIF technique with some other technique to gather EEDF data would allow for an accurate depiction of the  $T_e$ . The striation behavior predicted with simulation and theory can be observed

along the axis of our experimental setup; however, phenomena occurring radially that cause constriction and asymmetry are worth further investigation. It may also be relevant that our high voltage pulse drove enough current to push the experiments near the Pupp limit, which is why our data aligns well with computer simulations performed near the Pupp limit.<sup>11</sup> We have performed these measurements using laser-excited states without perturbing the plasma. We have introduced an analytic fit in the Appendix that allows quantitative interpretation of LCIF data without the need for running a complicated CRM. The observation of the wave transition (p to s) from 750 mTorr to 1 Torr contradicts the results from Ref. 27, which used light intensity to distinguish between the wave types. Because of the different operating conditions, it is difficult for us to directly compare our results, such as the phase differences between  $n_e$ , the 447:588 ratio, and light intensity, with previous studies. Future work could include studies matching the operating conditions of previous experiments and expanding the parameter space to investigate the diffuse to constricted transition in striated discharges. It would also be interesting to apply experimental EEDFs to our CRM and compare the results of temperature to the Maxwellian assumption, as mentioned above.

#### SUPPLEMENTARY MATERIAL

Videos of the striation propagation are provided as the supplementary material. These videos show the propagation of the striations in both the anode region and the cathode region.

#### **ACKNOWLEDGMENTS**

This material is based upon work supported by the NSF EPSCOR RII-Track-1 Cooperative Agreement No. OIA-1655280 and the U.S. Department of Energy, Office of Science, Office of Workforce Development for Teachers and Scientists, and the Office of Science Graduate Student Research (SCGSR) program. The SCGSR program is administered by the Oak Ridge Institute for Science and Education for the DOE under Contract No. DE-SC0014664. This work was supported by the U.S. Department of Energy, Office of Science, Office of Fusion Energy Sciences, under Award No. DE-SC0020232. Sandia National Laboratory is managed and operated by NTESS under DOE NNSA Contract No. DE-NA0003525. The authors would like to thank Dr. Ed Barnat at Sandia National Laboratory for his guidance and support in taking the measurements.

## **AUTHOR DECLARATIONS**

#### **Conflict of Interest**

The authors have no conflicts to disclose.

#### **Author Contributions**

**Z. K. White**: Conceptualization (equal); Data curation (equal); Formal analysis (equal). **R. P. Gott**: Data curation (equal); Methodology (equal). **B. Z. Bentz**: Formal analysis (equal); Methodology (equal).

**K. G. Xu**: Conceptualization (equal); Funding acquisition (equal); Project administration (equal).

#### **DATA AVAILABILITY**

The data that support the findings of this study are available within the article and its supplementary material.

# APPENDIX: RECOVERING $T_e$ AND $n_e$ FROM LIF AND LCIF INTENSITY RATIOS

Considering the set of helium LIF and LCIF intensity ratio curves as functions of  $T_{\rm eff}$  (eV) and  $n_e$  (cm<sup>-3</sup>) in Ref. 21, the 588:389 nm ratio is nearly linear with respect to  $n_e$ . In contrast, the 447:588 nm intensity ratio is non-linear with respect to both  $T_e$  and  $n_e$ . We find the following polynomial fits to these curves that can be used to interpret the LIF and LCIF ratio data:

$$x_1 = \log 10(588:389 \text{ nm}),$$
 (A1)

$$x_2 = \log 10(447:588 \text{ nm}),$$
 (A2)

$$\log 10(n_e) = 11.6851 + 0.8896x_1 - 0.0604x_1^2, \tag{A3}$$

$$T_e = 247.3 - 50.1x_1 + 507.6x_2 - 26.06x_1^2 - 49.3x_1x_2 + 412.3x_2^2$$

$$- 6.042x_1^3 - 24.03x_1^2x_2 - 12.04x_1x_2^2 + 163.7x_2^3 - 0.1135x_1^4$$

$$- 5.72x_1^3x_2 - 4.997x_1^2x_2^2 + 0.6136x_1x_2^3 + 31.38x_2^4$$

$$- 0.1417x_1^5 + 0.3324x_1^4x_2 - 1.689x_1^3x_2^2 + 0.3419x_1^2x_2^3$$

$$+ 0.2646x_1x_1^4 + 2.284x_2^5. \tag{A4}$$

The lower and upper bounds of  $n_e$  are about  $5 \times 10^8$  and  $5 \times 10^{12}$  cm<sup>-3</sup>. The lower and upper bounds of  $T_e$  are about 0.4 and 10 eV, respectively. The upper bound of helium gas pressure is about 5 Torr. The application of this analytic fit requires temporal LCIF measurements similar to those made here and in Ref. 21. These fits were found using the robust linear least-squares fitting method in MATLAB with 95% confidence bounds. The root mean squared error was less than 0.05 for each fit. Iteratively solving the CRM to generate the fitting data required hours of computational time on high performance computers.

# **REFERENCES**

- <sup>1</sup>L. Pekarek, "Ionization waves (striations) in a discharge plasma," Usp. Fiz. Nauk **94**(3), 463–500 (1968).
- <sup>2</sup> A. V. Nedospasov, "Striations," Sov. Phys. Usp. 11(2), 174 (1968).
- <sup>3</sup>P. S. Landa, N. A. Miskinova, and Y. V. Ponomarev, "Ionization waves in low-temperature plasmas," Sov. Phys. Usp. 23(12), 813–834 (1980).

- <sup>4</sup>K. F. Sodomsky, "Microwave measurements of moving striations in a DC glow discharge," J. Appl. Phys. **34**(7), 1860–1866 (1963).
- <sup>5</sup>S. F. Paik, J. N. Shapiro, and K. D. Gilbert, "Microwave absorption and density variation in moving striations," J. Appl. Phys. 35(9), 2573–2577 (1964).
- <sup>6</sup>D. A. Lee, P. Bletzinger, and A. Garscadden, "Wave nature of moving striations," J. Appl. Phys. **37**(1), 377–387 (1966).
- <sup>7</sup> A. B. Stewart, "Oscillating glow discharge plasma," J. Appl. Phys. **27**(8), 911–916 (1956).
- <sup>8</sup>N. L. Oleson and A. W. Cooper, "Moving striations," Phys. Rev. Lett. **105**(4), 1411–1412 (1957).
- <sup>9</sup> A. W. Cooper, "Experiments on the origin of moving striations," J. Appl. Phys. 35(10), 2877–2884 (1964).
- <sup>10</sup> V. I. Kolobov, "Striations in rare gas plasmas," J. Phys. D: Appl. Phys. 39, 4877 (2006).
- <sup>11</sup>R. R. Arslanbekov and V. I. Kolobov, "2-D simulations of striations in direct current glow discharges in argon," IEEE Trans. Plasma Sci. 33(2), 354–355 (2005).
- <sup>12</sup>V. I. Kolobov and R. R. Arslanbekov, "Simulation of electron kinetics in gas discharges," IEEE Trans. Plasma Sci. 34(3), 895–909 (2006).
- <sup>13</sup>R. R. Arslanbe and V. I. Kolobov, "Advances in simulations of moving striations in DC discharges of noble gases," Phys. Plasmas **26**(10), 104501 (2019).
- <sup>14</sup>J. P. Boeuf, "Ionization waves (striations) in a low-current plasma column revisited with kinetic and fluid models," Phys. Plasmas 29(2), 022105 (2022).
- <sup>15</sup>Y. B. Golubovskii, V. O. Nekuchaev, and A. Y. Skoblo, "Advances in the study of striations in inert gases," Tech. Phys. 59(12), 1787–1800 (2014).
- <sup>16</sup>L. D. Tsendin, "Electron kinetics in non-uniform glow discharge plasmas," Plasma Sources Sci. Technol. 4(2), 200–211 (1995).
- <sup>17</sup>V. I. Kolobov and V. A. Godyak, "Nonlocal electron kinetics in collisional gas discharge plasmas," IEEE Trans. Plasma Sci. 23(4), 503–531 (1995).
- <sup>18</sup>L. D. Tsendin, "Nonlocal electron kinetics in gas-discharge plasma," Phys.-Usp. 53(2), 133–157 (2010).
- <sup>19</sup>Y. B. Golubovskii, A. V. Siasko, D. V. Kalanov, and V. O. Nekuchaev, "Spatial and temporal formation dynamics of glow discharge constriction and stratification," Plasma Sources Sci. Technol. 27(8), 085009 (2018).
- <sup>20</sup>E. V. Barnat and V. I. Kolobov, "Nonmonotonic radial distribution of excited atoms in a positive column of pulsed direct current discharges in helium," Appl. Phys. Lett. **102**(3), 034104 (2013).
- <sup>21</sup>E. V. Barnat and K. Frederickson, "Two-dimensional mapping of electron densities and temperatures using laser-collisional induced fluorescence," Plasma Sources Sci. Technol. 19(5), 055015 (2010).
- <sup>22</sup>E. V. Barnat, "Multi-dimensional optical and laser-based diagnostics of low-temperature ionized plasma discharges," Plasma Sources Sci. Technol. 20(5), 053001 (2011).
- <sup>23</sup>B. R. Weatherford, E. V. Barnat, and J. E. Foster, "Two-dimensional laser collision-induced fluorescence measurements of plasma properties near an RF plasma cathode extraction aperture," Plasma Sources Sci. Technol. 21(5), 055030 (2012).
- <sup>24</sup>E. V. Barnat and B. R. Weatherford, "2D laser-collision induced fluorescence in low-pressure argon discharges," Plasma Sources Sci. Technol. 24(5), 055024 (2015).
- <sup>25</sup>V. Peřina, K. Rohlena, and T. Růžička, "Ionization waves (moving striations) in a low pressure helium discharge—Results of measurements compared with a direct solution of the electron Boltzmann equation," Czech. J. Phys. B **25**, 660 (1975).
- <sup>26</sup> K. Rohlena, T. Růžička, and L. Pekárek, "A theory of the low current ionization waves (striations) in inert gases," Czech. J. Phys. B **22**(10), 920–937 (1972).
- <sup>27</sup>V. Peřina, "Existence regions of ionization waves (moving striations) in helium, neon and argon," Czech. J. Phys. B **26**(7), 764–768 (1976).